Polymeric microellipsoids with programmed magnetic anisotropy for controlled rotation using low (≈10 mT) magnetic fields

Andrea Bonilla Brunner[1], Isabel Llorente García[2], Bumjin Jang[3], Midori Amano Patiño[4], Viraj Alimchandani[1] Bradley J. Nelson[3], Salvador Pané[3] and Sonia Contera[1*]

[1] Clarendon Laboratory, Department of Physics, University of Oxford, Parks Road, OX1 3PU, UK
[2] Department of Physics and Astronomy, University College London, Gower Street, London, WC1E 6BT

[3] Multi-Scale Robotics Lab (MSRL), Institute Swiss Federal Institute of Technology (ETH) Zurich, Tannenstrasse 3 CH-8092, CLA H9

[4] Institute for Chemical Research, Kyoto University, Uji, Kyoto 611-0011, Japan

*Corresponding author: Sonia.AntoranzContera@physics.ox.ac.uk

Abstract

Polymeric magnetic spherical microparticles are employed as sensors/actuators in lab-on-a-chip applications, small-scale robotics and biomedical/biophysical assays. Achieving controlled stable motion of the microparticles in a fluid environment using low intensity magnetic fields is necessary to achieve much of their technological potential; this requires that the microparticle is magnetically anisotropic, which is difficult to achieve in spheres. Here we have developed a simple method to synthesise anisotropic ellipsoidal microparticles (average eccentricity 0.60 ± 0.14) by applying a magnetic field during synthesis, using a nanocomposite of polycaprolactone (PCL) with Fe_3O_4 nanowires. The "microellipsoids" are thoroughly characterised using optical microscopy, scanning electron microscopy (SEM), transmission electron microscopy (TEM) and energy dispersive X-ray spectroscopy (EDX). Their suitability for magnetically controlled motion is demonstrated by analysing their rotation in low magnetic fields (0.1, 1, 5, 10 and 20 mT) at varying rotational frequencies (1Hz and 5Hz). The microellipsoids are able to follow smoothly and continuously the magnetic field, while commercial spherical particles fail to continuously follow the magnetic field, and oscillate backwards and forwards resulting in much lower average angular

speeds. Furthermore, only 23% of commercial particles analysed rotated at 1 Hz and 26% at 5 Hz, whereas 77% of our ellipsoidal particles rotated at 1 Hz, and 74% did at 5 Hz.

Keywords

Magnetic microparticles, polymeric microparticles, micromanipulation, programmed magnetic anisotropy, microfluidics, microrobots

1. Introduction

Magnetic polymer composites (MPCs) are widely used in microsystems and microrobotics as they simultaneously feature the processability and facile chemical functionalisation of polymers, and the possibility of using magnetic fields for actuation by exploiting the magnetic properties of the embedded nanostructures.[1-3]Magnetic fields are often preferred as external force generators due to their non-invasiveness, biological inertness, and better performance in comparison to other methods such as acoustic waves (including ultrasound) and electric fields.[4]

MPC-based microstructures can be used to perform tasks in handling and assembling small objects and biological molecules, or sensing physical, biological or chemical molecules or functions.[1, 5-7]In particular, MPCs shaped into spherical beads have been preferred as a favourite architecture for small-scale mechanical technologies due to the ease of fabrication, versatility and suitability for theoretical modelling. Spherical magnetic beads already play an important role in microfluidics; they can be made to link to target species and can be used for manipulation and/or detection in lab-on-a-chip systems[8-10] and protein and biomolecular purification and mixing. They are also used for generating and measuring forces at the micrometre scale in biophysical studies,[11-13] in torque-generating assays,[14] cellular mechanotransduction and microrheology, in magnetic twisting cytometry,[15, 16] in cellular, protein and nucleic acid manipulation in separation assays,[17] in immunoassays,[18] in magnetic flow cytometry,[19] in magnetic separation in lab-on-a-chip microfluidic systems,[20] in directed hyperthermia applications[11, 21] and targeted drug delivery.[22] Most applications use commercial spherical MPC microparticles consisting of a polymeric matrix that confines magnetic spherical superparamagnetic Fe_3O_4 nanoparticles (NPs).

The particular case of anisotropic microparticles has attracted a significant attention over the past two decades [23]. Particle anisotropy can be conveyed by fabricating non-spherical shapes and/or non-uniform surface properties. In both cases, their physical properties differ from those of isotropic microparticles, making them potentially useful for assembly e.g. colloidal substitutes for liquid

crystals and electrorheological fluids [24] [25], designing photonic crystals with novel symmetries, controlling suspensions' rheology [26] and suspensions' optical properties [27], stabilizing emulsions [28] and stabilizing foams [29], engineering of biomaterials [30] and colloidal composites [31]. Beyond building structure, anisotropic particles are also useful for engeneering dynamics at the microscale and actuation. In order to perform complex tasks and movements such as controlled rotation it is necessary to exert torque on the particle. One way of exerting magnetic torque on materials exhibiting magnetic moment is by controlling their shape anisotropy, which e.g. gives way to an easy-axis of magnetisation along the longest dimension in disks and rods. In a magnetic field, the most energetically favourable configuration is achieved when the easy axis of magnetisation aligns parallel to the direction of the applied field, producing rotation towards it [4, 32].

One of the main drawbacks of using spherical microparticles confining NPs is that they have relatively low shape anisotropy (as we demonstrate later in the results section), and require high magnetic fields to align all of the magnetic moments of the NPs inside of them [21]. To obtain a more controlled magnetic response several strategies aimed at programming magnetic anisotropy in the structure have been developed [2, 33]. Often these have involved top–down approaches such as inkjet printing [2] or photopatterning [33]. The applications of magnetic anisotropic particles include: (i) Fluid mixing in microfluidics and biosensing in small volumes of liquid: sample flow in small volumes and miniaturized channels is laminar [34]; and turbulent mixing between two liquids cannot be achieved. In lab-on-a-chip and microfluidic devices, it is crucial to attain a fast and adjustable mixing in applications in which several reactants or specimens are used. A magnetic microparticle that is able to rotate can be deployed in almost any environment to produce turbulence. This can find practical applications beyond mixing of reagents, for example, in extraction of specific micro/nano objects from a solution as they can be functionalized with specific molecules, proteins, bacteria or viruses. Turbulent flow can aid adsorption, prevents clustering of the target molecules/cells/microorganisms and from adhering to the container walls [35]. And (ii) biophysical assays: optical tweezers based on trapping polymer-based microbeads has revolutionized our understanding in motion in biological systems such as molecular motors, including the actions of ATP-synthases and bacterial flagellar motors. However, optical tweezers present drawbacks such as overheating of the samples. Magnetic tweezers are a promising alternative. However, they are currently used to manipulate commercial spherical microparticles, which prevents the advancement of the field, due to their intrinsic variability of their rotational behavior [14, 36].

Here we have synthesised magnetic nanocomposite microellipsoids based on a matrix of polycaprolactone (PCL) by a simple oil-in-water emulsion method. The polymer microellipsoids are formed in the emulsion in the presence of magnetite nanowires (Fe_3O_4), which are trapped in the

particle matrix. During the synthesis, DC magnetic fields are used to align the nanowires and create magnetic (shape) anisotropy. The particles are thoroughly characterised using optical microscopy, scanning electron microscopy (SEM), transmission electron microscopy (TEM) and energy dispersive X-ray spectroscopy (EDX). Furthermore, the superior rotation properties at low magnetic field intensity in comparison to commercially available microparticles is demonstrated using rotating magnetic fields with field strengths of 0.1, 1, 5, 10 and 20 mT, at varying rotation frequencies (1Hz and 5Hz).

2. Materials and Methods

2.1 Nanowire synthesis

Fe_3O_4 nanowires were prepared by hydrolysis of Fe^{3+} [37]. Briefly, a solution consisting of 420 mM $FeCl_3 \cdot 4H_2O$, 210mM $FeSO_4 \cdot 7H_2O$ and 1M $(NH_2)_2CO$ (all chemicals from Sigma Aldrich, UK) was prepared with deoxygenated Milli-Q water (Nitrogen flow for 30 minutes) and stirred for 10 minutes. The solution was then added to a Teflon flask and placed in an autoclave reactor. A 0.45T NdFeB magnet (First4magnets, UK) was positioned in the bottom of the autoclave to induce nanowire growth on the easy axis [38]. The reactor was placed in an oven at 130°C for 6 hours. After this time, the reactor was allowed to cool down at room temperature overnight. The resulting black magnetic dispersion was washed 3 times with deoxygenated water and freeze dried for 24 hours.

2.2 Microellipsoid synthesis

Microellipsoids were synthesised by using the oil-in-water emulsion method, as illustrated in Fig. 1. The oil phase contained luperox (benzoyl peroxide, Sigma Aldrich) (2.5% w/v), which acted as the initiator of PCL crosslinking, dissolved in dichloromethane at 0.5 mM. Synthesised Fe_3O_4 nanowires (described above) were dispersed in the PCL solution at a concentration of 0.5% (w/v) which is at least 20 times smaller concentration than commercial particles (≈10 to 39% of Fe_3O_4 content depending on the manufacturer). In order to achieve a homogeneous dispersion of nanowires in the oil phase, the solution was sonicated in a water bath for 5 minutes.

The water phase consisted of soluble poly(vinyl alcohol) (PVA, Sigma Aldrich, UK) (1.5% w/v) as a non-surfactant stabilizer. The oil phase was emulsified by adding it dropwise into the water phase while stirring at 3,000 rpm (MS1 Minishaker IKA, UK), and emulsified for 10 minutes at this speed. Liquid agar (1% w/v) was immediately added, mixed for 3 minutes and settled in the freezer at -20°C for 10 minutes. Liquid agar was used to immobilize the microellipsoids, preventing them to

collect back together into a bigger oil phase droplet, hence allowing them to harden individually. A static magnetic field of 0.25 T was applied during hardening to modify the orientation of the nanowires embedded within the polymeric structure. The gel was aged at room temperature overnight to allow particle hardening. Finally, microellipsoids were cleaned and sorted by size using density gradient centrifugation with a glucose column, at 3,000 rpm for 7 minutes. The smallest microellipsoid (those corresponding to the first layer of the gradient) were used for this study. The microellipsoids were rinsed 3 times with ultrapure deionized (DI) water (Millipore MilliQ, UK) and kept at 4°C. The dimensions distribution of the ellipsoid are given in the Fig. 2S in the supplement.

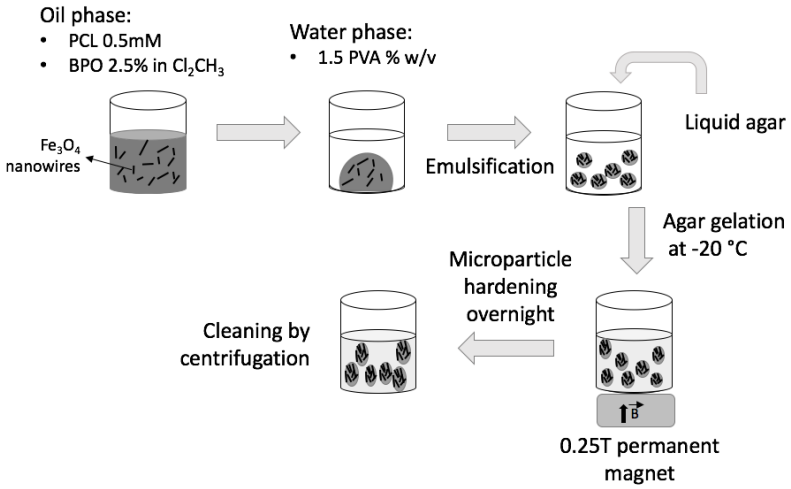

Figure 1. Schematic representation of the oil-in-water emulsion synthesis of the microellipsoids. The oil phase contains benzoyl peroxide (2.5% w/v) and 0.5 mM PCL dissolved in dichloromethane with 0.5% Fe_3O_4 nanowires dispersed. The water phase consists of PVA 1.5% w/v. The oil phase was emulsified into the water phase by stirring. Liquid agar (1% w/v) was immediately added and settled at -20 °C during microellipsoid hardening in the presence of a static magnetic field of 0.25 T. Particles were left at room temperature overnight to allow PCL hardening while inducing orientation of the nanowires and creating the ellipsoidal shape.

2.3 Microellipsoid characterisation. TEM and SEM imaging

The microstructure and phase of the nanowires and the microellipsoids were analysed by TEM on a FEI Talos F200X instrument operated at 200 keV acceleration voltage. Both, TEM and scanning TEM (STEM) operation modes of the instrument were used for the study. STEM studies were performed in the high angle annular dark field (HAADF STEM) imaging mode and accompanied by elemental content analysis using energy dispersive spectroscopy EDX STEM. STEM and EDX STEM studies were carried out using a 0.8 nm probe size.

SEM images were acquired by a secondary electron detector in a Zeiss ULTRA 55 apparatus. The sample was dispersed on a Si wafer and dried.

2.4 Rotation experiments

The rotational motion of microellipsoids was characterised using a commercial magnetic actuation system (MFG-100-i, Magnebotix, Switzerland) mounted on an optical microscope (Olympus IX, Olympus). The magnetic actuation system consists of 4 pairs of solenoid coils which allow 3D manipulation of micrometer-size magnetic objects. Experiments were carried out in ultrapure DI water deionized water (Millipore MilliQ) applying various magnetic field amplitudes (0.1, 1, 5, 10 and 20 mT) for fields rotating at two different frequencies (1 and 5 Hz). Commercial superparamagnetic spherical polystyrene beads (nominal diameter: 2.0-2.9 μm, SPHERO™ Magnetic Particles: PM-20) were assessed as a control. Particle motion was recorded using a CCD camera (SCA 1400, Basler) at 30 frames per second (fps).

2.5 Image processing to analyse the rotation of the microellipsoids.

A suite of image processing algorithms for single particle rotational tracking was custom-written in Matlab to quantitatively extract the orientation of all particles in each acquired video sequence. The program automatically detects all microellipsoids in each video frame via intensity thresholding. This operation results in a binary image with connected regions, i.e., masks, for each particle on top of a zero background. The ellipse that best fits the shape of each particle mask shape is then found to extract the particle centre-of-mass, major and minor axis lengths and orientation angle of the major axis with respect to the horizontal image axis. The eccentricity is calculated for each microellipsoid using the obtained major and minor axis lengths. Single-particle tracking is then achieved by linking particles found on subsequent frames. The linking decision is based on comparing the pair-wise distances between each particle on a given frame and all particles on the previous frame and choosing the assignment with the smallest pair-wise distance. After all tracking assignments are made, the result is a set of particle trajectories for each video analysed, so that the orientation angle of the particles as a function of time can be analysed.

The angular velocity of all the rotating colloids during uniform rotation (excluding oscillations) was calculated for particles that completed at least one 360° turn. Additionally, the

185 effective frequency of rotation (number of full turns per second) of the colloids subjected to small
186 field intensities (0.1 and 1 mT) was also quantified.

187

188 ## 3. Results and discussion

189 ### 3.1 Structural characterisation

190 Microellipsoids were synthesised as described in the materials and methods. The average
191 microparticle yield is approximately 7 % for the particle size competent to this study (2-3 µm). This
192 value is so low since the emulsification process lacks of particle size control, resulting in a high
193 particle size dispersion.

194 Fig. 2 (a) shows two typical microellipsoids imaged by SEM displaying a clear ellipsoidal shape with
195 different eccentricities (ε). ε represents how ellipsoidal a particle is (ε = 1 for infinite rods and ε = 0
196 for spheres), and is calculated using the formula:

197 $$\varepsilon = \sqrt{\frac{a^2-b^2}{a^2}}\ , \quad 0< \varepsilon <1\ , \qquad [1]$$

198 for prolate ellipsoids with semiaxes a and b.

199 PCL microparticles fabricated without nanowires and in the absence of a magnetic field using
200 this method present a spherical shape (Fig. A.1, supplementary material).

201 TEM was used to identify the arrangement of the Fe_3O_4 nanowires within the particle (Fig. 2 (b)). The
202 presence of a magnetic field during synthesis results in the formation of clusters (shown in Fig. 2 (c))
203 which eventually determines the final ellipsoidal shape of the particle.

204 The images indicate that the magnetic field applied during the synthesis is not sufficient to align all
205 the individual nanowires and overcome forces arising from the interaction between polymers and
206 nanowires during crosslinking and colloid hardening. The formation of nanowire clusters could also
207 be the result of attractive interactions between nanowires before the magnetic field was applied, or
208 pre-clustering due to rotational forces during emulsification and particle formation from the oil
209 phase. Despite this clustering, the magnetic field is sufficiently strong to orient clusters of wires so
210 that the resulting particles exhibit an ellipsoidal shape. As a control, we performed the same
211 synthesis protocol in the absence of a magnetic field (supplementary Materials A, Fig. A2); in this
212 case the most of the particles presented a spherical shape, highlighting the role of the magnetic field
213 aligning the clusters during synthesis.

Future experiments regarding the fabrication of microparticles with nanoparticles embedded (instead of nanowires or nanoparticles attached to the surface) in the presence of an external magnetic field during hardening, could also, in principle, produce ellipsoidal shapes since nanoparticles could also align to the field producing stretching of the particle. *In general, the elongated shape of a magnetic composite in the presence of a magnetic field is energetically more favourable.* Previous work by Faraudo et al. [39] has shown that superparamagnetic microspheres can become aligned in certain conditions in fluid environments, where a key parameter is the magnetic coupling coefficient between the particles. However, due to their shape isotropy, a large magnetic gradient is needed for alignment even in water (10–30 T m^{-1}). It is therefore reasonable to assume that producing alignment of nanoparticles in a polymeric matrix would require even larger magnetic fields that are not practical for a facile synthesis methods. Indeed, our results show that even with nanowires that are much larger and can align much easier than nanoparticles in a magnetic field, total alignment is not possible with the relatively low magnetic fields used in our work. However, the magnetic fields used in our paper succeed to produce ellipsoids by alignment of clusters of nanowires, which leads to the success of our initial purpose: to create anisotropic magnetic particles with a simple synthesis method.

In order to quantify ε for the microellipsoids, a and b were measured from optical microscopy images of the particles in solution as described above (Fig. B.1). The distribution of ε is shown in Fig. 2 (d) for a total of 159 colloids analysed, confirming that the synthesis method clearly leads to ellipsoidal particles.

Finally, in Fig. 2 (e) we show a TEM analysis of individual nanowires. EDX analysis of the nanowires embedded within the polymeric PCL lattice is also shown in Fig. 2 (e), EDX allow us to identify that the nanowires consist of iron oxide, iron content is depicted in red and oxygen in green (see Fig. C.1 for details).

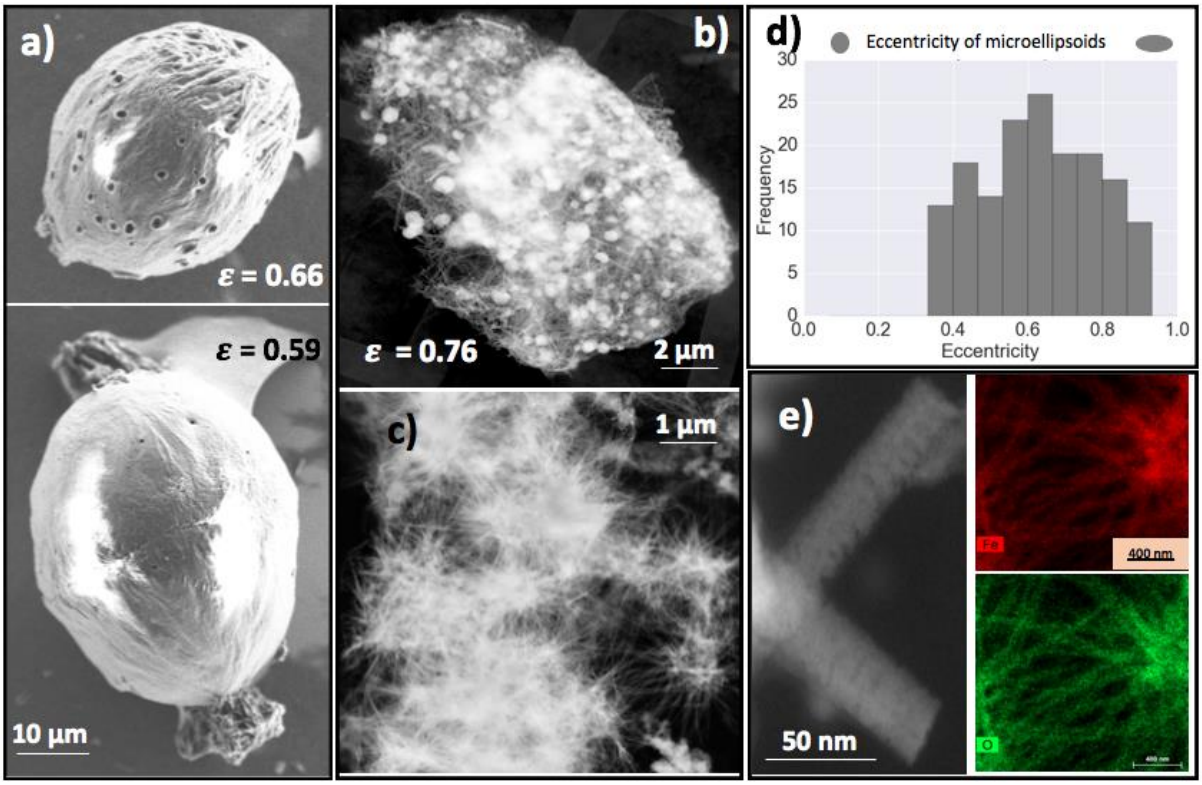

Figure 2. a) SEM images of synthesised magnetic ellipsoidal particles with different eccentricities ε. b) TEM images of microellipsoids showing the nanowire structure embedded within the polymer matrix. c) Nanowire cluster formation due to the presence of a magnetic field during microparticle hardening. d) Histogram of ε values of the microellipsoids. e) TEM image of synthesised Fe_3O_4 nanowires and EDX analysis showing the structural composition of the nanowires (supplementary data, Fig. S3).

3.2 Angular velocity of the ellipsoidal colloids and comparison with commercial spherical colloids

In order to evaluate the performance of the microparticles, we monitored and analysed their movement subject to rotating magnetic fields, using the automatic method described in the materials section. Two examples of the application of the method are given in Fig. 3. Fig. 3 (a) displays a typical time sequence for the rotation of one of the microellipsoids in the presence of a 10 mT magnetic field rotating at a frequency of 1 Hz. Fig. 3 (c) shows a sequence for a different particle and a 10 mT magnetic field rotating at 5 Hz. The initial orientation angle detected is between -90 degrees and +90 degrees, and smooth particle rotation with constant angular velocity is indicated by the clear periodicity and linearity of the angle versus time (blue traces in Figs. 3 (b) and 3 (d)).

Further processing of the angle is carried out by automatically detecting orientation jumps in the data and assuming anti-clockwise rotation to generate a monotonically increasing positive angle (red traces in Figs. 3 (b) and 3 (d)). This can be fitted to a line (solid black lines in Figs. 3 (b) and 3 (d)) to

obtain from the slope the angular velocity and frequency of rotation of the microparticle. For particles that display uneven rotation with non-constant angular velocity, jumps or angle oscillations, only linear segments (detected automatically in the angle-versus-time data) of approximately constant angular velocity are fitted to a line. An average rotation frequency is then calculated as the mean of the frequencies corresponding to all rotation segments in these cases. Particle trajectories with less than 10 frames and rotation segments with less than 5 frames are excluded from the analysis. Only isolated particles are analysed (particles that clump together into large clusters are discarded for the analysis).

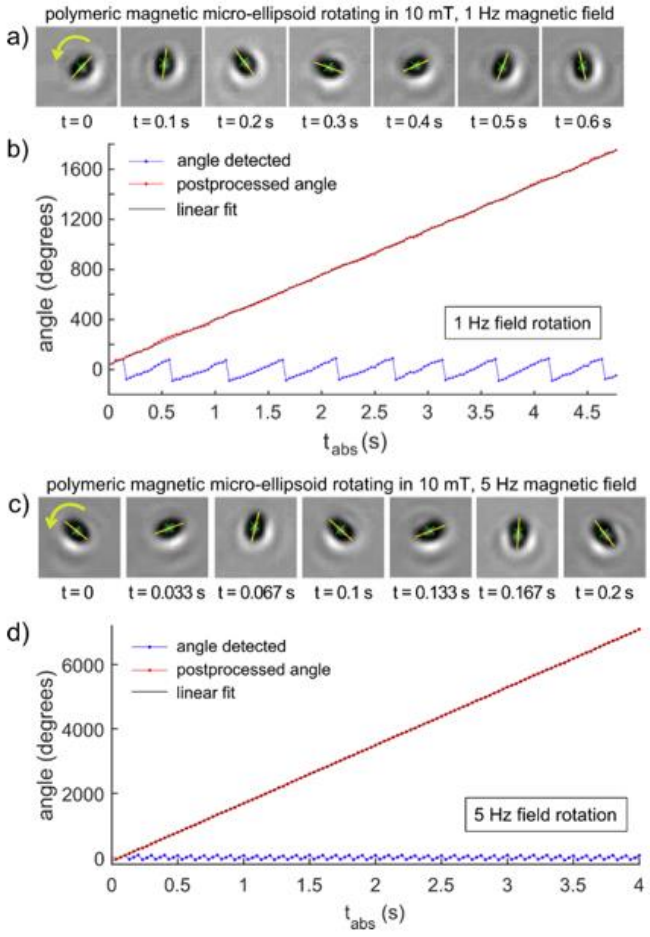

Figure 3. Quantitative extraction of particle rotation angle and frequency via image processing. a) Sequence of image frames acquired for one of our polymeric magnetic microellipsoids rotating in a 10 mT, 1 Hz rotating magnetic field. Every third frame acquired is shown. Yellow lines indicate the angle found for the particle. Green crosses indicate the found centre-of-mass. The rotation of the field and particle is counter-clockwise as indicated by the rotation arrow on the first frame. b) Orientation angle versus time for a ~ 5-second-long rotation sequence corresponding to the particle shown in a). The fit of the post-processed angle (see text) yields a particle rotation frequency of (0.996±0.001) Hz, very close to the field-rotation frequency. c) Rotation time sequence for one of our particles in the presence of a 10 mT, 5 Hz rotating magnetic field. Every frame acquired is shown. d) Orientation versus time for the particle rotating in the 5 Hz field. The linear fit yields a particle rotation frequency of (4.995±0.001) Hz.

Note that the depicted particle presents a selected case where smooth rotation following the rotation of the magnetic field is achieved, yet some particles deviate from this ideal performace. Figure. 4 shows the dispersion (error bars in histogram) of angular velocities of all the studied colloids (that completed a 360º turn and rotated individually).

Using this procedure (fits of linear segments of orientation angle vs time), we calculated the angular velocity of the all the colloids in the presence of a rotating magnetic field. We used field intensities 0.1 mT, 1 mT, 5 mT, 10 mT, 20 mT and rotational frequencies of 1 Hz and 5 Hz. A total of 400 particles were analysed for theresults presented in Fig. 4. Although over a hundred particles were analysed for each condition, only data for a relatively small number of particles was useful for quantitative analysis, since only particles able to perform at least a complete 360° turn were considered (including particles that performed backwards rotation movements and oscillations). The graphs indicate the fraction of particles that fulfil this criterion. It is important to note that a larger number of ellipsoidal particles were able to rotate individually (32.6% of particles agglomerated) in comparison to the majority of the commercial particles where the majority of particles (67.2%) agglomerated, making it harder to get a good sample number of rotating particles. The analysis of these uniform rotation segments in Fig. 4 shows that the performance of the ellipsoidal particles in terms of measured rotation frequency is similar to that of the commercial spherical particles, considering the measurement uncertainties. However, careful analysis of the data shows that commercial microparticles present a more irregular behaviour, especially at low magnetic fields (which are more interesting from an application point of view). Significantly, only 23 % of commercial particles analysed were able to individually complete at least a full 360° turn at 1 Hz, with this fraction being 26 % at 5 Hz on average over all magnetic field strengths. For instance, at the lowest magnetic field strength of 0.1mT, out of 10 commercial spherical particles assessed, only 4 completed at least a full turn at 1Hz, and none at 5Hz. In comparison, our ellipsoidal particles displayed a clearly superior performance at all field strengths, with 77 % completing at least a full turn at 1 Hz, and 74 % at 5 Hz on average.

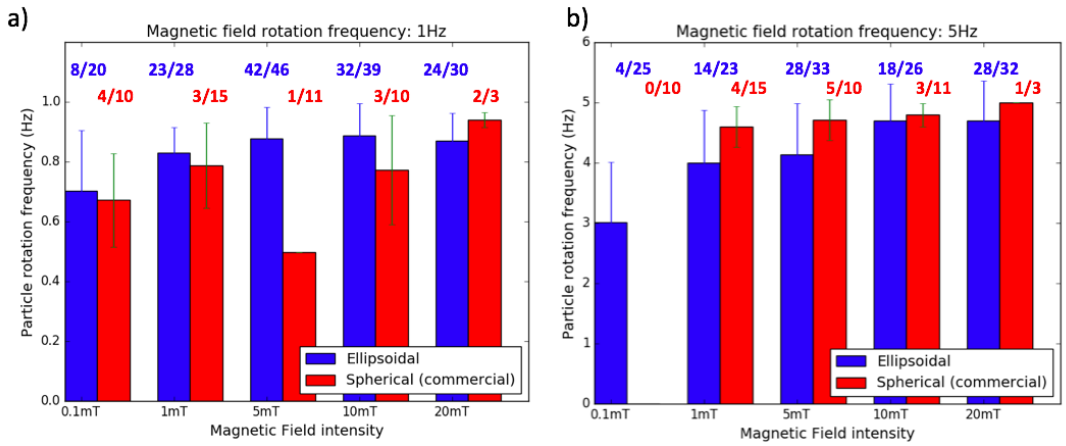

306

307 Figure 4. Angular velocities of colloids calculated with the procedure shown in Fig. 3 (fitting linear
308 segments of orientation angle vs time and averaging to obtain a mean particle rotation frequency) at
309 different intensities of the rotating magnetic field at (a) 1 Hz and (b) 5 Hz field rotation frequencies.
310 Ellipsoidal particles are shown in blue and commercial spherical particles are shown in red. Fractions at
311 the top of the bars show the numbers of particles that completed at least one full 360° cycle divided by
312 the total number of particles.

313

314 However, the previous analysis is not sufficient to evaluate the comparative performance of
315 the particles, especially at low intensities of the magnetic field (0.1 mT, 1 mT). At low field strengths,
316 the microellipsoids are able to smoothly follow the rotating magnetic field (see Video 1 in
317 supplementary information), whereas the commercial spherical microparticles do not follow the
318 field rotation smoothly and display oscillations in orientation, backwards rotation and jumps in
319 orientation (see Video 2 in supplement). Fig. 5 shows a comparison of two representative examples
320 of commercial microparticles and microellipsoids subject to a 1 mT, 1Hz magnetic field (Videos 1, 2
321 corresponding to these images are available in supplementary material).

322 Fig. 5 (a) shows the reasonably smooth rotation of the microellipsoid, whereas Fig. 5(b)
323 shows the angle versus time for the commercial spherical particle, which displays oscillations and
324 back and forth rotations. Although the spherical microparticle returns to its minimum orientation
325 angle (-90 degrees) as many times as the microellipsoid does, the microsphere does not actually
326 perform the same number of total turns as the microellipsoid. This is because the microsphere in
327 fact returns to the minimum angle by rotating backwards (green arrows) in some instances (see
328 video 2 in the supplement and Fig. 5(b)). Hence, the total number of turns per second is reduced to
329 0.48 Hz for the spherical microparticle, compared to 0.98 Hz for the microellipsoid (Fig. 5(a)).

330

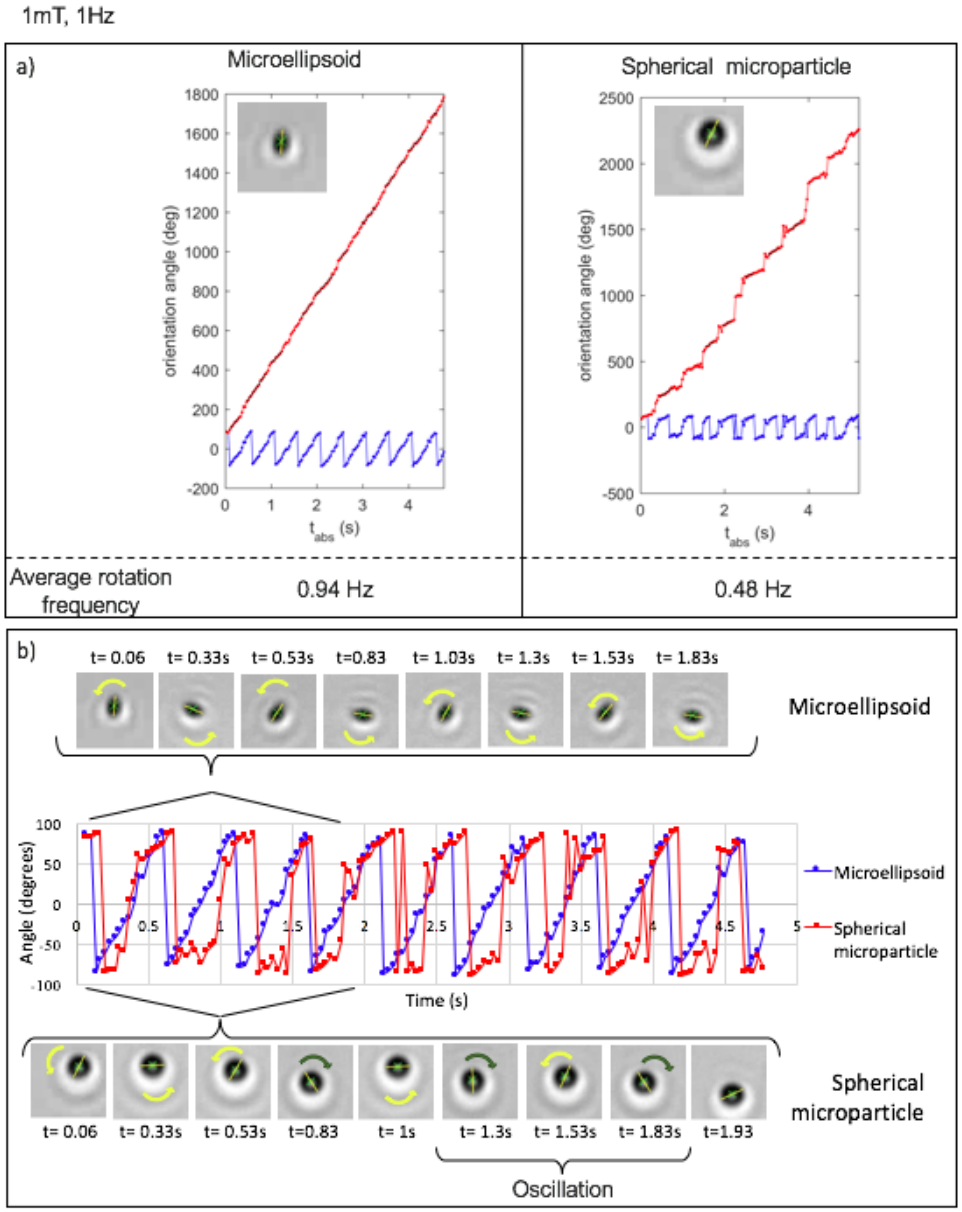

Figure 5. Comparison of spherical (commercial) microparticles and microellipsoids as they are actuated by a 1mT magnetic field rotating at 1Hz. (a) Representative examples of ellipsoidal (left) and spherical (right) colloid orientation angle vs. time graphs. At the bottom of each graph, the corresponding average rotation frequency (full rotation turns per second) is displayed for each case (see text). (b) Orientation angle of ellipsoidal (blue) and spherical (red) colloids vs. time corresponding to the same data depicted in (a). A sequence of images of the particle rotating at different times is included for the microellipsoid (top) and the spherical microparticle (bottom). Arrows depict the rotation direction of the, displaying oscillations and movement in the same (yellow arrows)/opposite (green arrows) direction to the applied magnetic field for the commercial spherical microparticles (corresponding Videos 1 and 2 are given in supplementary material). It is important to note that in the frames (t=0.83, 1s and 1.83 and 1.93s), the microparticle turned to 0 degrees by rotating backwards. Some oscilation (back and forth change of the angle) is also observed.

Since, at low magnetic fields, smooth rotation is not achieved for the spherical microparticles (Fig. 5 (b)), it is more useful, in order to compare their performance, to quantify the total number of full rotations per unit time observed from the videos. Fig. 6 shows violin plots of the number of full rotations per second for all the commercial microparticles and microellipsoids that completed at least one full turn, subject to a rotating field of (a) 0.1 mT and (b) 1 mT. These plots show the probability density of the data in order to visualise -in a more explicit way-, the amount of particles rotating a number of times per second and their distribution in each of the cases. Each side of the middle lines in each plot is a kernel density estimation and the distribution of the data. The wider regions of the violin plot show a higher probability of the component of the population to take a given value. Violin plots in figure 6 were smoothed by a kernel density estimator evaluated at 40 points and were implemented using the Python.

For the 0.1mT, 1 Hz field, the microellipsoids rotated with a mean number of full rotations per second of (0.35 ± 0.19) Hz, while this value was (0.22 ± 0.01) Hz for the commercial microspheres. For the 0.1 mT, 5 Hz field, the microellipsoids' average number of full rotations per second was (0.29 ± 0.15) Hz, while no commercial microparticle managed to perform a single full turn.

For the 1 mT, 1 Hz field, the average number of full rotations per second was (0.61 ± 0.27) Hz for the microellipsoids and (0.26± 0.13) Hz for the commercial particles. It is important to observe that the standard deviations for all field strengths and frequencies are larger for the microellipsoids than for the commercial particles. This is mainly due to a higher spread on rotation performance and a much larger number of assessed individual particles that complete at least one full turn for the microellipsoids compared to the commercial microparticles. This may be due to the different sizes of the microellipsoids and to variations in their magnetic (shape) anisotropy and/or inconsistent distribution of Fe_3O_4 nanowires within the particles due to the lack of nanoscale control of the fabrication process.

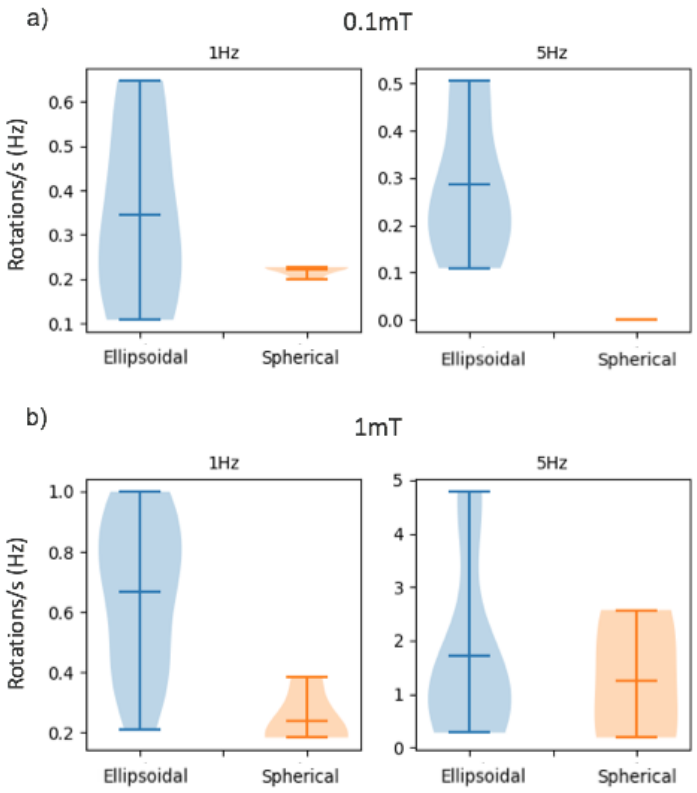

Figure 6. Violin plots of the average number of full rotations per second for commercial spherical microparticles (orange) and microellipsoids (blue) in the presence of (a) 0.1 mT and (b) 1 mT magnetic fields rotating at 1 Hz (left) and 5 Hz (right).

Taking all the recorded particles into account (microellipsoids and spherical microparticles), different behaviours were observed: from completely static particles -probably stuck to the bottom of the container- to particles rotating only a few degrees back and forth, particles completing only slightly less than a full 360 degree turn and particles moving backwards a few degrees and then forwards in an oscillating manner (only spherical microparticles). Behaviour deviating from smooth rotation in the direction of the field was mainly observed at the lowest intensities of the field and for the commercial spherical microparticles. These are a result of the particles not reaching the necessary energy to turn when trying to align with a rotating magnetic field. On the other hand, at higher intensities of the field, spherical particles agglomerate more.

These results demonstrate that the synthesised ellipsoidal colloids outperformed the spherical commercial microparticles at following the rotation of low magnetic fields. It is reasonable to hypothesise that the relatively strong magnetic torque experienced by ellipsoids in the external rotating magnetic fields (as compared to that exerted on the microspheres) is mainly due to global shape effects which create a deviation of the magnetization vector inside ellipsoids with respect to the instantaneous direction of the applied field. This significant magnetic torque should allow a

smooth rotation of ellipsoids. Local magnetic susceptibility anisotropy effects cannot be completely ruled out as they can arise from complex effects due to the arrangement of the nanowires and their interactions within the microelliosoids [40]. But the smooth rotation (even at low fields) points towards a isotropic magnetic susceptibility within the ellipsoids, at least in the times and length scales probed here. The lower average effective rotation frequency measured for the commercial spherical microparticles and the appearance of oscillations and jumps in rotation are possibly due to their lower shape anisotropy (Fig. S.2 in the supplementary material). It is also possible that stochastic heterogeneities of the iron oxide distribution in the microspheres can lead to fluctuations of the magnetic torque and thus to fluctuations of the rotation speed of the particles. Furthermore, the thickness of the nanoparticle layer covering the spherical polystyrene core in the commercial particles might not be totally homogeneous for all the particles, producing some of the variability of their performance. It is also likely that the higher content of magnetic material for the commercial particles (approximately 20 times higher than in the microellipsoids) makes them heavier and more likely to adhere to the surface of the underlying substrate. The higher mass should also affect their moment of inertia.

4. Conclusions

We report the synthesis of anisotropic, ellipsoidal microparticles following a novel, simple procedure based on the oil-in-water emulsion method. The microellipsoids are based on a lattice of biocompatible PCL with embedded Fe_3O_4 nanowires; the ellipsoidal shape is achieved by using a magnetic field during synthesis. In order to evaluate the comparative advantage that ellipsoidal particles offer with respect to existing commercial spherical particles for magnetic control, we compared the rotational dynamics for both types of particles in magnetic fields with varying intensities (0.1, 1, 5, 10 and 20 mT) and rotational frequencies (1Hz and 5Hz).

Both commercial and ellipsoidal particles are able to follow smoothly magnetic fields at the higher field strengths (10 and 20 mT). However, at low field strengths (0.1 and 1 mT), commercial spherical particles present a lower effective average rotation frequency than the ellipsoidal particles, due to the occurrence of oscillations and jumps in rotation. A large proportion of commercial microparticles do not complete a single 360° turn. In total, only 23% of commercial particles analysed rotated for 1Hz fields and 26% for 5 Hz fields, whereas 77% of our ellipsoidal particles rotated at 1 Hz, and 74% did at 5 Hz. Furthermore, the number of individual commercial spherical microparticles able to rotate at higher field strengths (5, 10 and 20 mT) is very small (Fig. 4), owing to

aggregation of the particles with increasing field strengths. On the other hand, our microellipsoids were capable of full rotation individually at higher field strengths avoiding aggregation.

Our results show the superior rotation performance of the ellipsoidal particles in rotating magnetic fields in comparison to spherical commercial particles as expected from their intrinsic shape anisotropy, even though their magnetic material content is at least 20 times smaller than that of the commercial particles. The ellipsoidal shape makes the fabricated microellipsoids amenable to simple computational tracking and to theoretical calculations and modelling, which are key considerations for designing and fine-tuning future applications. The method presented here can be easily substituted for other top-down approaches such as 3D printing (size restricted to printer resolution), electrospraying [41], continuous-flow microfluidics [42, 43], soft lithography [44], etc. These methods could be fine-tuned by adapting them with other polymeric matrices and they present advantages over emulsification methods such as a better nanowire alignment, reduction of nanowire cluster formation -due to lack of rotational forces present during emulsification-, monodisperse size and ellipsoidal shape, control over the particle hardening process, uniform application of magnetic field, microparticle magnetic response optimisation, etc. However, these methods require infrastructure and expertise, which make them more unpractical for scaling-up as compared to the simple method presented in this paper.

Our simple fabrication and computational tracking method, along with a high (magnetic) shape anisotropy that allows for a better particle control using lower magnetic fields is than existing methods based on commercial microparticles, makes our ellipsoids good candidates for many of the applications mentioned in the introduction section, such as biophysical studies, magnetic tweezers, microfluidics, nucleic acid and protein manipulation, microrheology, torque-generating assays, magnetically directed drug delivery, etc.

Acknowledgements

The author(s) would like to acknowledge networking support by the COST Action CA16122. ABB gratefully acknowledges support from a Mexican government CONACYT scholarship and support by a STSM Grant from COST Action CA16122.

Data availability

All the experimental data will be deposited and made available through the Oxford Research Archive portal (https://ora.ox.ac.uk/).

References

[1] W.-l. Chiang, C.-j. Ke, Z.-x. Liao, S.-y. Chen, F.-r. Chen, C.-Y. Tsai, Y. Xia, H.-W. Sung, Pulsatile Drug Release from PLGA Hollow Microspheres by Controlling the Permeability of Their Walls with a Magnetic Field, Small 8(23) (2012) 3584-3588.

[2] O. Ergeneman, S. Gervasoni, B. Ozkale, P. Fatio, V.J. Cadarso, B.J. Nelson, Inkjet printed superparamagnetic polymer composite hemispheres with programmed magnetic anisotropy, Nanoscale 6(18) (2014).

[3] J. Thévenot, H. Oliveira, O. Sandre, S. Lecommandoux, Magnetic responsive polymer composite materials, Chemical Society Reviews 42 (2013) 7099-7116.

[4] R.M. Erb, J.J. Martin, R. Soheilian, C. Pan, J.R. Barber, Actuating Soft Matter with Magnetic Torque, Advanced Functional Materials 26 (2016) 3859-3880.

[5] A. Butykai, A. Orbán, V. Kocsis, D. Szaller, S. Bordács, E. Tátrai-Szekeres, L.F. Kiss, A. Bóta, B.G. Vértessy, T. Zelles, I. Kézsmárki, Malaria pigment crystals as magnetic micro-rotors: Key for high-sensitivity diagnosis, Scientific Reports 3 (2013) 1-10.

[6] O. Ergeneman, G. Chatzipirpiridis, J. Pokki, M. Marin-Suárez, G.A. Sotiriou, S. Medina-Rodriguez, J.F.F. Sanchez, A. Fernandez-Gutiérrez, S. Pane, B.J. Nelson, In vitro oxygen sensing using intraocular microrobots, IEEE Transactions on Biomedical Engineering 59(12 PART2) (2012) 3104-3109.

[7] S. Tottori, L. Zhang, F.M. Qiu, K.K. Krawczyk, A. Franco-Obregon, B.J. Nelson, Magnetic Helical Micromachines: Fabrication, Controlled Swimming, and Cargo Transport, Adv Mater 24(6) (2012) 811-816.

[8] A. Rida, M.A.M. Gijs, Manipulation of Self-Assembled Structures of Magnetic Beads for Microfluidic Mixing and Assaying, Analytical Chemistry 76(21) (2004) 6239-6246.

[9] N. Pamme, Magnetism and microfluidics, Lab on a chip 1 (2006).

[10] V. Reenen, D. Jong, D. Toonder, M.W.J. Prins, Integrated lab-on-chip biosensing systems based on magnetic particle actuation : a comprehensive review Lab on a Chip, Lab on a chip 12 (2014).

[11] L. Chen, H. Zhang, L. Li, Y. Yang, X. Liu, B. Xu, Thermoresponsive hollow magnetic microspheres with hyperthermia and controlled release properties, Journal of Applied Polymer Science · (September 2017) (2015).

[12] E.K. Paluch, C.M. Nelson, N. Biais, B. Fabry, J. Moeller, B.L. Pruitt, C. Wollnik, G. Kudryasheva, F. Rehfeldt, W. Federle, Mechanotransduction : use the force(s), BioMed Central Biology (2015) 1-14.

[13] W.J. Polacheck, C.S. Chen, Measuring cell-generated forces : a guide to the available tools, Nature methods 13(5) (2016) 415-423.

[14] M.M. Van Oene, L.E. Dickinson, B. Cross, F. Pedaci, J. Lipfert, N.H. Dekker, Applying torque to the Escherichia coli flagellar motor using magnetic tweezers, Scientific Reports 7 (2017) 1-11.

[15] M. Puig-de-morales, M. Grabulosa, J. Alcaraz, J. Mullol, G.N. Maksym, J.J. Fredberg, D. Navajas, M. Grabulosa, J. Al, J. Mullol, G.N. Maksym, J. Jeffrey, D. Navajas, Measurement of cell microrheology by magnetic twisting cytometry with frequency domain demodulation, Journal of Applied Physiology 91 (2001) 1152-1159.

[16] N. Wang, J.P. Butler, D.E. Ingber, Mechanotransduction Across the Cell Surface and Through the Cytoskeleton, Science 260(May) (1993) 1124-1128.

[17] C. Sun, H. Hassanisaber, R. Yu, S. Ma, S.S. Verbridge, C. Lu, Paramagnetic Structures within a Microfluidic Channel for Enhanced Immunomagnetic Isolation and Surface Patterning of Cells, Scientific reports (July) (2016) 1-9.
[18] H.-s. Lin, J.R. Carey, The Design and Applications of Nanoparticle Coated Microspheres in Immunoassays, Journal of Nanoscience and Nanotechnology 14(1) (2014) 363-377.
[19] A. Vila, V.C. Martins, A. Chícharo, C. Rodriguez-abreu, A.C. Fernandes, F.A. Cardoso, S. Cardoso, J. Rivas, P. Freitas, Customized Design of Magnetic Beads for Dynamic Magnetoresistive Cytometry, IEEE TRANSACTIONS ON MAGNETICS 50(11) (2014) 18-21.
[20] L. Clime, B.L. Drogoff, T. Veres, Dynamics of Superparamagnetic and Ferromagnetic Nano-Objects in Continuous-Flow Microfluidic Devices, IEEE TRANSACTIONS ON MAGNETICS 43(6) (2007) 2929-2931.
[21] J. Faraudo, J.S. Andreu, C. Calero, J. Camacho, Predicting the Self-Assembly of Superparamagnetic Colloids under Magnetic Fields, Advanced Functional Materials 26 (2016) 3837-3858.
[22] S.-w. Cao, Y.-j. Zhu, M.-y. Ma, L. Li, L. Zhang, Hierarchically Nanostructured Magnetic Hollow Spheres of Fe 3 O 4 and γ -Fe 2 O 3 : Preparation and Potential Application in Drug Delivery, Journal of Physical Chemistry 112(6) (2008) 1851-1856.
[23] V.R. Dugyala, S.V. Daware, M.G. Basavaraj, Shape anisotropic colloids: synthesis, packing behavior, evaporation driven assembly, and their application in emulsion stabilization, Soft Matter 9(29) (2013) 6711-6725.
[24] V.N. Paunov, O.J. Cayre, Supraparticles and "Janus" particles fabricated by replication of particle monolayers at liquid surfaces using a gel trapping technique, Adv Mater 16(9-10) (2004) 788-+.
[25] J.W. Kim, R.J. Larsen, D.A. Weitz, Synthesis of nonspherical colloidal particles with anisotropic properties, J Am Chem Soc 128(44) (2006) 14374-14377.
[26] R.G. Larson, The structure and rheology of complex fluids, Oxford University Press, New York ; Oxford, 1999.
[27] M.I. Mishchenko, J.W. Hovenier, L.D. Travis, Light scattering by nonspherical particles : theory, measurements, and applications, Academic Press, San Diego ; London, 2000.
[28] A.D. Dinsmore, M.F. Hsu, M.G. Nikolaides, M. Marquez, A.R. Bausch, D.A. Weitz, Colloidosomes: Selectively permeable capsules composed of colloidal particles, Science 298(5595) (2002) 1006-1009.
[29] R.G. Alargova, D.S. Warhadpande, V.N. Paunov, O.D. Velev, Foam superstabilization by polymer microrods, Langmuir 20(24) (2004) 10371-10374.
[30] S.C. Glotzer, M.J. Solomon, Anisotropy of building blocks and their assembly into complex structures, Nature Materials 6(8) (2007) 557-562.
[31] P.F. Noble, O.J. Cayre, R.G. Alargova, O.D. Velev, V.N. Paunov, Fabrication of "hairy" colloidosomes with shells of polymeric microrods, J Am Chem Soc 126(26) (2004) 8092-8093.
[32] R.S.M. Rikken, R.J.M. Nolte, J.C. Maan, J.C.M.V. Hest, D.A. Wilson, P.C.M. Christianen, Manipulation of micro- and nanostructure motion with magnetic fi elds, Soft Matter 10 (2014) 1295-1308.
[33] J. Kim, S.E. Chung, S.-e. Choi, H. Lee, J. Kim, S. Kwon, Programming magnetic anisotropy in polymeric microactuators, Nature Materials 10(10) (2011) 747-752.
[34] V. Hessel, H. Lowe, F. Schonfeld, Micromixers - a review on passive and active mixing principles, Chem Eng Sci 60(8-9) (2005) 2479-2501.
[35] A. van Reenen, A.M. de Jong, J.M.J. den Toonder, M.W.J. Prins, Integrated lab-on-chip biosensing systems based on magnetic particle actuation - a comprehensive review, Lab on a Chip 14(12) (2014) 1966-1986.

[36] M.M. van Oene, L.E. Dickinson, F. Pedaci, M. Kober, D. Dulin, J. Lipfert, N.H. Dekker, Biological magnetometry: torque on superparamagnetic beads in magnetic fields, Phys Rev Lett 114(21) (2015) 218301.
[37] S. Lian, E. Wang, Z. Kang, Y. Bai, L. Gao, M. Jiang, C. Hu, L. Xu, Synthesis of magnetite nanorods and porous hematite nanorods, Solid State Communications 129 (2004) 485-490.
[38] M. Wang, H.J. Jin, D.L. Kaplan, G.C. Rutledge, Mechanical properties of electrospun silk fibers, Macromolecules 37(18) (2004) 6856-6864.
[39] J. Faraudo, J.S. Andreu, J. Camacho, Understanding diluted dispersions of superparamagnetic particles under strong magnetic fields: a review of concepts, theory and simulations (vol 9, pg 6654, 2013), Soft Matter 9(48) (2013) 11709-11709.
[40] J.J. Wang, Y. Song, X.Q. Ma, L.Q. Chen, C.W. Nan, Static magnetic solution in magnetic composites with arbitrary susceptibility inhomogeneity and anisotropy (vol 117, 043907, 2015), J Appl Phys 119(6) (2016).
[41] H. Lee, S. An, S. Kim, B. Jeon, M. Kim, I.S. Kim, Readily Functionalizable and Stabilizable Polymeric Particles with Controlled Size and Morphology by Electrospray, Scientific Reports 8 (2018).
[42] L.A. Shaw, S. Chizari, M. Shusteff, H. Naghsh-Nilchi, D. Di Carlo, J.B. Hopkins, Scanning two-photon continuous flow lithography for synthesis of high-resolution 3D microparticles (vol 26, pg 13543, 2018), Opt Express 26(11) (2018) 14718-14718.
[43] D. Dendukuri, D.C. Pregibon, J. Collins, T.A. Hatton, P.S. Doyle, Continuous-flow lithography for high-throughput microparticle synthesis, Nature Materials 5(5) (2006) 365-369.
[44] J.J. Guan, A. Chakrapani, D.J. Hansford, Polymer microparticles fabricated by soft lithography, Chem Mater 17(25) (2005) 6227-6229.

Supplementary materials

A. Sphericity of colloids synthesised by oil-in-water emulsion with/without nanowires and with no applied magnetic field during hardening.

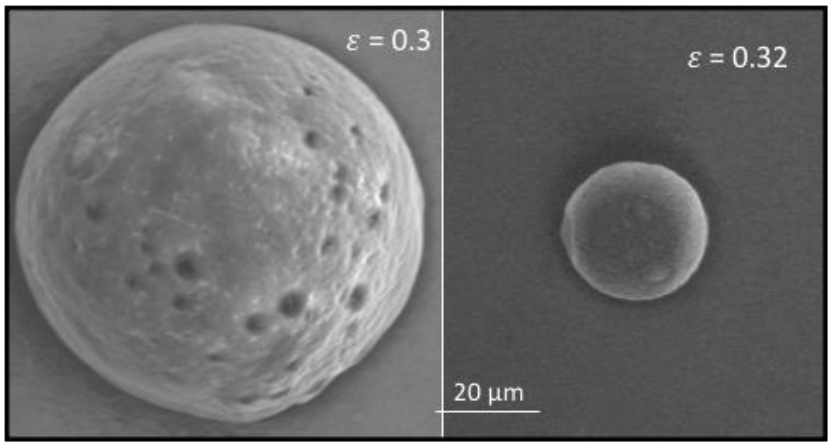

Figure A.1 SEM images of PCL colloids without nanowires and without magnetic field applied during the synthesis showing higher sphericity.

Figure A.1 shows colloids consisting of PCL synthesised by the same oil-in-water emulsion method as described in the microellipsoid synthesis section (oil phase consisting of Luperox 2.5% w/v and 0.5 mM PCL dissolved in dichloromethane; water phase PVA 1.5% w/v; no nanowires embedded). These particles show higher sphericity in comparison to the ellipsoidal microparticles described in the main text (with 0.5% w/v magnetic Fe_3O_4 nanowires embedded in the polymeric matrix and aligned in the presence of a 0.25T magnetic field during hardening).

Similarly, Figure A.2 shows an optical microscopy image of microparticles synthesised as described in the microellipsoid synthesis section without a magnetic field present during hardening as a control.

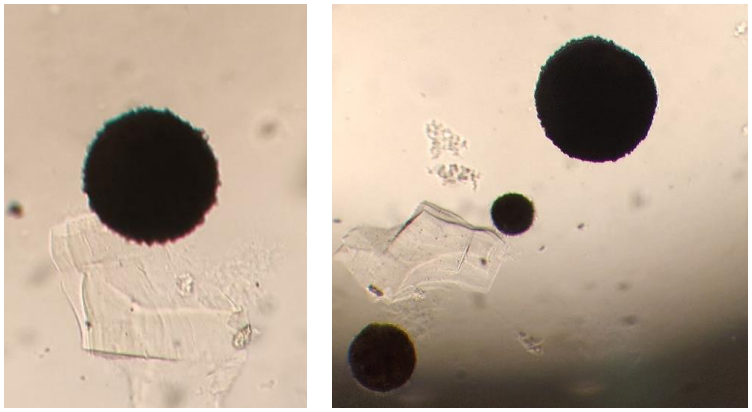

Figure A.2. Optical microscopy image of microparticles of polycaprolactone and Fe_3O_4 that were synthesized in the absence of a magnetic field, presenting a spherical shape, with ε= 0.4±0.2.

B. Major and minor axis lengths of ellipsoidal and commercial spherical microparticles

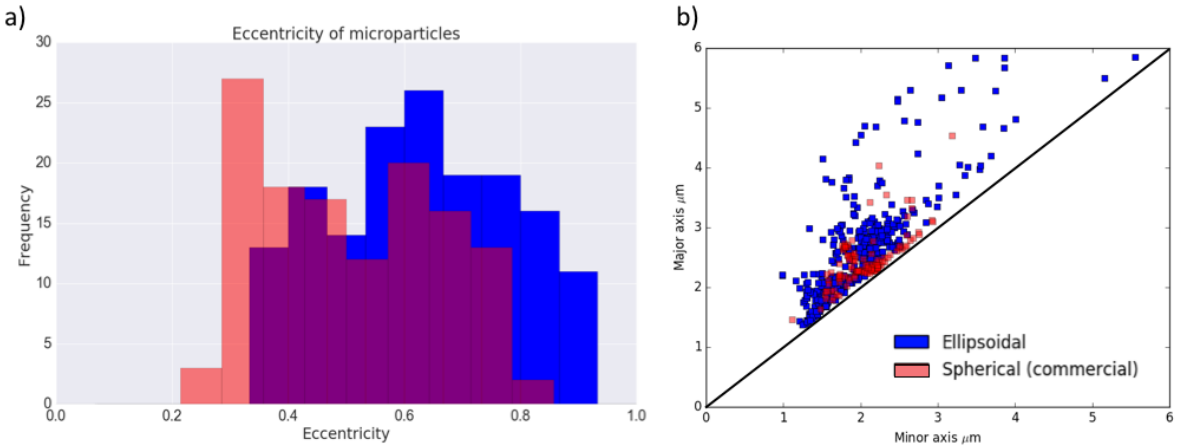

Figure B.1 a) Histogram plot of the eccentricity of the commercial microparticles (red) against the ellipsoidal synthesised microparticles (blue). b) Minor vs. major axis of all of the analysed microparticles.

Figure B.1 a) shows a histogram of the eccentricity of both the ellipsoidal (blue) and the spherical (commercial) particles (red), calculated from the measured microparticle dimensions as explained in the image processing section. Eccentricity tends to cero with higher sphericity of the particle. It is apparent that the eccentricity of the commercial particles is smaller than that of the synthesised ones, with a mean value of the particle major axis $2a = 2.48 \pm 0.55$ μm and $\varepsilon = 0.40 \pm 0.15$ for the commercial particles and $2a = 2.68 \pm 1.10$ μm and $\varepsilon = 0.60 \pm 0.14$ for the particles synthesised in this paper.

Figure B.1 b), shows a scatter plot of the major vs minor axis for all the analysed particles (synthesised particles in blue, commercial in red).

C. TEM/ EDX Fe_3O_4 nanowire structural composition analysis.

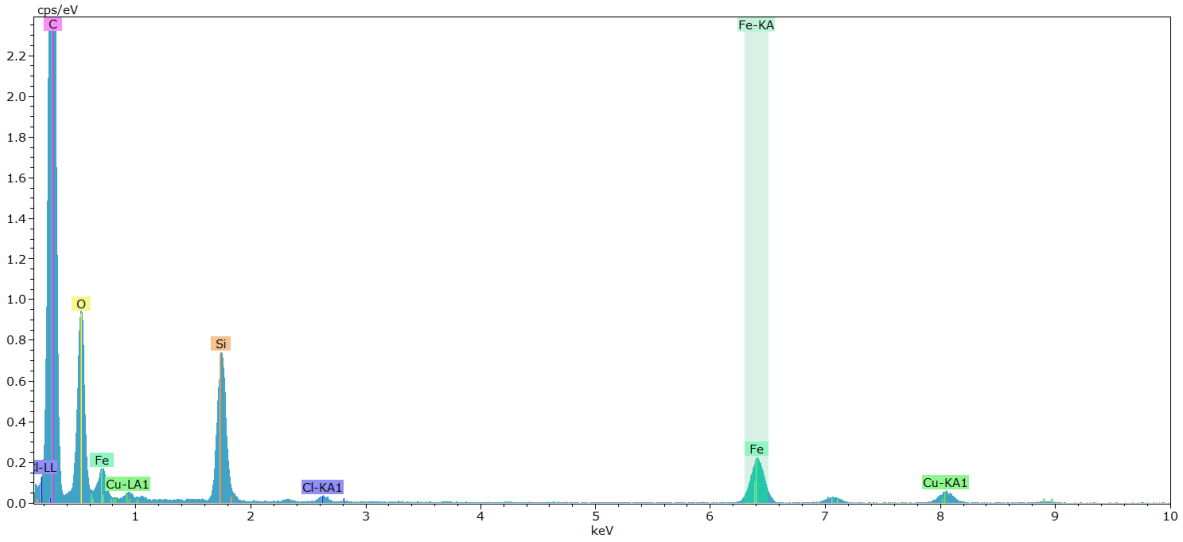

Figure C.1 EDX spectrum of Fe_3O_4 nanowires synthesised as described in the materials and methods and shown in figure 2 (Results: Structural characterisation section).

The EDX analysis of the nanowires embedded in the PCL lattice shown in figure C.1 in the structural characterisation results section confirms the presence of Fe (0.72 and 6.40 keV), O (0.53 keV) related to the Fe_3O_4 nanowires and C (0.27 keV) related to the polymeric PCL lattice.

D. Nanowire magnetic characterisation: superconducting quantum interference device (SQUID) Measurements

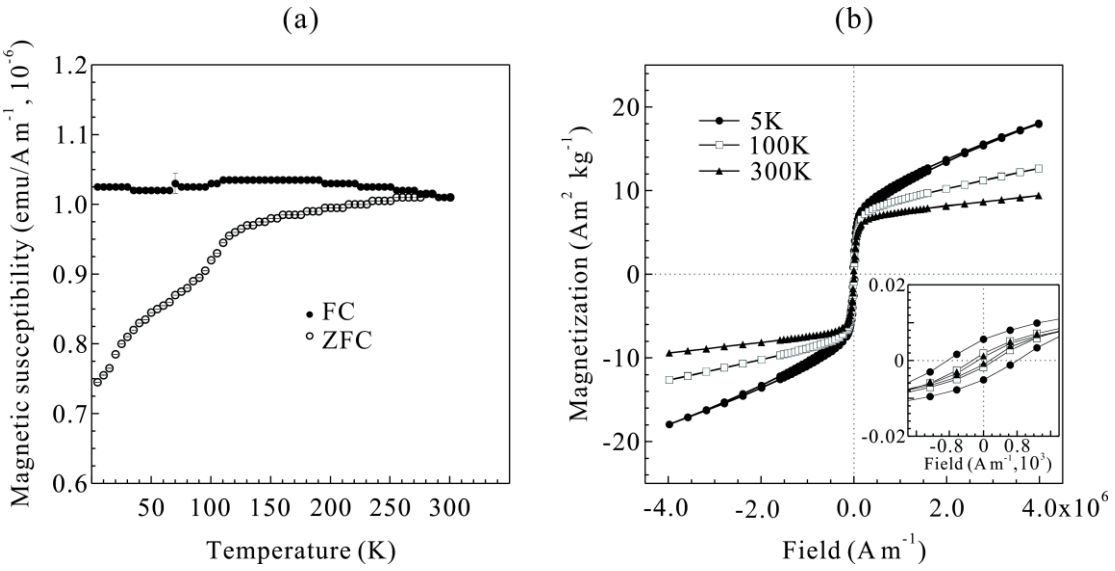

Figure D1. (a) Zero field cooled (ZFC) and field-cooled (FC) magnetic susceptibility curves for a sample of Fe_3O_4 nanowires measured using a field of 796 A m^{-1} in the range 5 ≤ T (K) ≤ 300. (b) The magnetization isotherms at T = 5, 100, 300 K and field range -3.98 ≤ H (x10^6 A m^{-1}) ≤ 3.98. Inset: enlargement of the coercive zone.

In figure D1 a) we can see a feature at T ≈ 120 K both in the zero field cooled (ZFC) and field cooled (FC) curves that corresponds well to the Verwey transition for Fe_3O_4 samples in the nanoscale [3] although no temperature in the measurement window seems to correspond to the blocking temperature (TB). The ZFC and FC curves diverge throughout the whole range of temperatures measured suggesting that the TB is greater than 300 K.

A value of TB greater than 300 K is in agreement with the coercivity observed in the M/H isotherms shown in Figure D1 b). As shown in the inset, the coercive field HC decreases upon heating from 5 to 100 K, from 21.52x103 to 6.68 x103 A m^{-1} (where 1/4π A m^{-1} = 1x10^{-3} Oe). However, at 300 K, an HC of 3.35x103 A m^{-1} is still observed. An HC of approximately 0 A m^{-1} would be expected from a superparamagnetic behaviour. Nevertheless, the observed value HC = 3.35x10^3 is in good agreement with previously reported values of HC for Fe_3O_4 nanowires and nanoparticles at 300 K. [3],[2].

The saturation magnetization (MS) was not reached during the collection of the M/H isotherms even at an applied field of 3.98x106 A m^{-1} (5 T). The maximum magnetizations registered at the maximum applied field are 18.05, 12.66 and 9.41 Am2 Kg^{-1} (1 Am^2 Kg^{-1} = 1 emu g^{-1}) for the isotherms at 5, 100 and 300 K respectively. Remanent saturation magnetization values of 10.22, 7.87 and 6.90 Am^2 Kg^{-1} can be extracted from extrapolation of M versus 1/H plots. These rather small values for the magnetization can be explained form the random orientation of the Fe_3O_4 nanowires during our measurements [4]. The magnetic domains in the Fe_3O_4 nanowires sample can be found oriented parallel, perpendicular and even antiparallel with respect to the applied magnetic field, thus hindering the observed overall magnetic moment [4].

The shape of the ZFC and FC curves is also consistent with previous reports in the literature for Fe_3O_4 nanowire arrays of diameters in the range of 100 to 200 nm [4]. The breadth of both curves can be explained from a distribution of sizes of the nanowires, which leads to a distribution of values for the magnetic susceptibility as the temperature approaches TB.

Interactions between nanowires can shift HC to smaller or higher values depending on local ordering and orientation of the easy axis [1].

References

[1] Castellanos-Rubio, I.; Insausti, M.; Garaio, E.; Gil de Muro, I.; Plazaola, F.; Rojo, T.; Lezama, L. Nanoscale 2014, 12, 7542.

[2] Han, R.; Li, W.; Pan, W.; Zhu, M.; Zhou, D.; Li, F. Sci. Rep. 2015, 4 , 7493.

[3] Yang, J. B.; Xu, H.; You, S. X.; Zhou, X. D.; Wang, C. S.; Yelon, W. B.; James, W. J. J. Appl. Phys. 2006, 99 , 08Q507.

[4] Zhang, L.; Zhang, Y. J. Magn. Magn. Mater. 2009, 321, L15.

Conflict of Interest Statement

Polymeric microellipsoids with programmed magnetic anisotropy for controlled rotation using low (≈10 mT) magnetic fields

Andrea Bonilla Brunner
Isabel Llorente García
Bumjin Jang
Midori Amano Patiño
Viraj Alimchandani
Bradley J. Nelson
Salvador Pané
Sonia Contera

The authors listed above declare no competing financial interest.